

Inter-patient ECG Arrhythmia Classification with LGNs and LUTNs

Wout Mommen, Lars Keuninckx, Paul Detterer, Achiel Colpaert and Piet Wambacq, *Senior Member, IEEE*

Abstract—Deep Differentiable Logic Gate Networks (LGNs) and Lookup Table Networks (LUTNs) are demonstrated to be suitable for the automatic classification of electrocardiograms (ECGs) using the inter-patient paradigm. The methods are benchmarked using the MIT-BIH arrhythmia data set, achieving up to 94.28% accuracy and a $\text{j}\kappa$ index of 0.683 on a four-class classification problem. Our models use between 2.89k and 6.17k FLOPs, including preprocessing and readout, which is three to six orders of magnitude less compared to SOTA methods. A novel preprocessing method is utilized that attains superior performance compared to existing methods for both the mixed-patient and inter-patient paradigms. In addition, a novel method for training the Lookup Tables (LUTs) in LUTNs is devised that uses the Boolean equation of a multiplexer (MUX). Additionally, rate coding was utilized for the first time in these LGNs and LUTNs, enhancing the performance of LGNs. Furthermore, it is the first time that LGNs and LUTNs have been benchmarked on the MIT-BIH arrhythmia dataset using the inter-patient paradigm. Using an Artix 7 FPGA, between 2000 and 2990 LUTs were needed, and between 5 to 7 mW (i.e. 50 pJ to 70 pJ per inference) was estimated for running these models. The performance in terms of both accuracy and $\text{j}\kappa$ -index is significantly higher compared to previous LGN results. These positive results suggest that one can utilize LGNs and LUTNs for the detection of arrhythmias at extremely low power and high speeds in heart implants or wearable devices, even for patients not included in the training set.

Index Terms—AI accelerators, Artificial intelligence, Backpropagation, Edge AI, Logic gates, Neuromorphic computing, Ultra low power

I. INTRODUCTION

The World Health Organization (WHO) states that globally in 2025, the main cause of death is so-called cardiovascular diseases (CVDs) [1]. Each year, about 17.9 million people die of CVDs [1]. Hence, measures need to be taken for early detection or monitoring of such CVDs. Heart implants or even wearables could obtain such information, provided that these battery-operated hardware use very low power. Generally, the MIT-BIH arrhythmia data set [2] is used as a first step

This research received funding from the Flemish Government under the “Onderzoeksprogramma Artificiële Intelligentie (AI) Vlaanderen” programme.

W. Mommen, L. Keuninckx, P. Detterer, A. Colpaert and P. Wambacq are with imec, Kapeldreef 75, 3001 Leuven, Belgium (e-mail: wout.mommen@imec.be; lars.keuninckx@imec.be; paul.detterer@imec.be; achiel.colpaert@imec.be; piet.wambacq@imec.be).

W. Mommen and P. Wambacq are with the Vrije Universiteit Brussel, Pleinlaan 2, 1050 Elsene Belgium.

to benchmark different technologies or algorithms for ECG arrhythmia classification, irrespective of the power usage [3], [4], [5], [6]. However, if these algorithms are envisioned to run on small embedded devices such as pacemakers, where replacing the battery is not desired, care should be taken regarding the power and energy consumption of these algorithms.

Quantization and pruning of artificial neural networks have been used in the past to increase power and energy efficiency of these algorithms [7]. A next approach is to use a Spiking Neural Network to do the arrhythmia classification [8], [9]. To further reduce energy consumption, researchers have explored non-conventional computing systems. For example, the use of Monostable Multivibrator (MMV) networks has been shown to improve power efficiency and is straightforward to implement in hardware [10]. These MMV networks use simple digital timers as their basic element. To further extend this trend, researchers have explored reducing the network elements even further, and state-of-the-art research has demonstrated that networks of digital logic gates can be trained to tackle a wide range of tasks. These Deep Differentiable Logic Gate Networks (LGNs) [11] are constructed from the optimal 2-input logic gate network configuration with randomly chosen fixed connections, utilizing a given dataset and traditional backpropagation techniques. Similarly, networks built with simple Lookup Tables (LUTs) have been proposed in literature under different names: LUTNet [12], [13], LogicNets [14], NullaNet [15], PolyLUT [16], NeuralLUT [17], Differentiable Weightless Neural Networks (DWNNs) [18] and Walsh-Assisted Relaxation for Probabilistic Look-Up Tables (WARP-LUTs) [19]. For clarity, in this work, we will use the term Lookup Table Network (LUTN) since this best represents its essence. Although a LUT element consists of multiple logic gates, it offers two advantages over LGNs. Firstly, a LUT is a reconfigurable element that enables a single LUTN architecture to execute different functionalities. Secondly, a LUT can have more than two input ports, allowing for more complex neuron functions. To create a LUTN for a specific application, two methods have been presented: on one side, a regular neural network can be converted into a LUTN using a multitude of techniques [12], [13], [14], [15], [16], [17], on the other side, a LUTN can be trained directly [18], [19]. The first solution allows for conventional neural network training, but the final accuracy is lower and the number of LUTs is quite high, while the second method adapts the training algorithm, allowing for

high accuracy and a much fewer LUTs. Questions remain open on whether a LUTN can be used for efficient arrhythmia classification, what potential data preprocessing would be required, and how to efficiently train these LUT networks for this type of application.

In this work, to address the aforementioned open questions, we propose an ECG classification system using LUTNs by implementing a novel training method and preprocessing method. The contributions of this work can be summarized as follows:

- 1) The first exploration of the MIT-BIH arrhythmia data set on the LGNs using the inter-patient paradigm.
- 2) The first usage of the LUTNs on the MIT-BIH data set, showing that these types of networks are also suitable for arrhythmia classification.
- 3) A new method for training the LUTs in LUTNs by using the Boolean equation of a MUX.
- 4) The first time using rate coding on the LGNs and LUTNs, showcasing a better performance on the MNIST, Fashion-MNIST and MIT-BIH data set using the LGNs.
- 5) An alternative preprocessing for the LGNs, showing an increased performance compared to the previous preprocessing techniques using both the mixed-patient and inter-patient paradigms.

II. RELATED WORK

SNNs [20] are often used as energy-efficient AI models for a wide range of applications, including ECG arrhythmia classification. Mao *et al.* [8] benchmarks the MIT-BIH data set on an SNN, achieving an accuracy of 93.67% using 0.3 μ J per inference on a chip with a leakage power of 1.14 μ W. Yan et al. [9] trained a two-stage CNN on the MIT-BIH data set. The first classifier acts as a wake-up system to determine if there is a normal heartbeat or an arrhythmia and the second classifier determines the type of arrhythmia. Both CNNs were converted to rate-coded SNNs, achieving an accuracy of 90.00 % and a $j\kappa$ index of 0.636. The estimated power to run these SNNs back to back is 77 mW.

Deep Differentiable Logic Gate Networks (LGNs) were first introduced by Petersen *et al.* [11]. An LGN is a network of randomly connected 1-input and 2-input logic gates. The gate-layers are connected to each other using randomly chosen connections that remain fixed during training. The gate type, on the other hand, is learned using backpropagation by creating a linear combination of the operations f_i of all 16 gates and learning the corresponding coefficients w_i . One can apply the softmax function on the coefficients, essentially learning a discrete probability distribution p_i over all possible gates. The output of the gate is the activation and is given by [11]

$$a = \sum_{i=0}^{15} p_i \cdot f_i(x_0, x_1) = \sum_{i=0}^{15} \frac{e^{\mathbf{w}_i}}{\sum_j e^{\mathbf{w}_j}} \cdot f_i(x_0, x_1). \quad (1)$$

The real-valued logic operations f_i used in this formula can be found in Table I. Since (1) is differentiable,

backpropagation can be used to learn the gate-type. At the end of training, the gate-type with the highest probability is chosen for each superposition. This final network can be used for inference. After the final layer of the network, one groups the outputs of the different gates, where each group corresponds to one class, and counts the number of 1's for each group. The highest value of these group sums (i.e. population counters) determines the predicted class. During training, these population count values are converted to probabilities using a softmax function with temperature T , a hyperparameter of the model. Apart from feedforward LGNs, it is also possible to create recurrent [21] and convolutional architectures [22]. All of these architectures exhibit very low power consumption at a high throughput, as they are essentially networks of 2-input logic gates. It is also possible to train the connections of these networks [23], in that way, a much smaller network can be used to perform the same task with a similar performance. Apart from the classical LGNs, Gumbel LGNs [24] have been proposed, which use Gumbel noise to decrease training time, increase the number of *used* neurons, and decrease the discretization gap.

TABLE I: The index of summation i , corresponding binary operation, truth table and real-valued logic operation f_i . [11]

i	Operation	00	01	10	11	f_i
0	False	0	0	0	0	0
1	$x_0 \wedge x_1$	0	0	0	1	$x_0 x_1$
2	$\neg(x_0 \Rightarrow x_1)$	0	0	1	0	$x_0 - x_0 x_1$
3	x_0	0	0	1	1	x_0
4	$\neg(x_0 \Leftarrow x_1)$	0	1	0	0	$x_1 - x_0 x_1$
5	x_1	0	1	0	1	x_1
6	$x_0 \oplus x_1$	0	1	1	0	$x_0 + x_1 - 2x_0 x_1$
7	$x_0 \vee x_1$	0	1	1	1	$x_0 + x_1 - x_0 x_1$
8	$\neg(x_0 \vee x_1)$	1	0	0	0	$1 - (x_0 + x_1 - x_0 x_1)$
9	$\neg(x_0 \oplus x_1)$	1	0	0	1	$1 - (x_0 + x_1 - 2x_0 x_1)$
10	$\neg x_1$	1	0	1	0	$1 - x_1$
11	$x_0 \Leftarrow x_1$	1	0	1	1	$1 - x_1 + x_0 x_1$
12	$\neg x_0$	1	1	0	0	$1 - x_0$
13	$x_0 \Rightarrow x_1$	1	1	0	1	$1 - x_0 + x_0 x_1$
14	$\neg(x_0 \wedge x_1)$	1	1	1	0	$1 - x_0 x_1$
15	True	1	1	1	1	1

Lookup Table Networks (LUTNs) [18] are similar to LGNs, but instead of using logic gates as “neurons”, Lookup Tables (LUTs) are employed. These LUTNs can be seen as a generalization of LGNs, in the sense that a LUT transforms an n -bit input into one binary output, while a logic gate transforms a 2-bit input into one binary output. Hence, a 2-LUT is equivalent to an LGN. Due to the increased complexity of the “neurons”, an n -input LUT can learn exponentially more functions than a logic gate. Namely, the number of functions scales as 2^{2^n} . As can be seen from Table II, this means that the number of possible learnable functions for a single LUT increases exponentially as the number of inputs increases. The most basic building block of an FPGA is the 6-LUT. Thus, having the ability to learn a network of 6-LUTs on a specific data set can lead to very efficient implementations of AI algorithms on FPGAs. Additionally, due to the high complexity (compared to logic gates) of these 6-LUTs, it is expected that we will need fewer neurons and hence less global interconnect for chip

implementations. Consequently, chips can be smaller and routing easier when using 6-LUTs compared to logic gates. Along with reconfigurability, this is the primary motivation for switching from LGNs to LUTNs.

Some research has already been conducted on LUTNs. Wang *et al.* [12], [13] take a pruned XNOR-Net [25] and convert it to a network of LUTs, called LUTNet. This network still includes activation functions and accumulation operations. Umuroglu *et al.* introduce LogicNets [14], which are sparse quantized neural networks converted into networks of LUTs. They manage to map an artificial neuron with limited and quantized inputs (X) and outputs (Y) to an $X:Y$ logical LUT, which can be implemented in FPGAs using their underlying hardware building blocks, such as 6:1 or 5:2 physical LUTs. The transformation from neuron to logical LUT eliminates the need for multiply and accumulate operations, making the computation more efficient. Due to the transformation from logical LUT to physical LUTs, the final AI model only consists of physical LUTs and their connectivity. NullaNet [15] also converts neurons to logical LUTs, but these logical LUTs are converted to sum-of-products terms and are next converted to logic gates using a logic synthesis tool, optimizing for area, delay, and power consumption. PolyLUT [16] is similar to LogicNets, since it also maps neurons to logical LUTs to physical LUTs, but their neuron contains multivariate polynomials instead of a linear transformation, such that fewer physical LUTs are needed for the same accuracy. NeuraLUT [17] builds further on PolyLUT, modelling entire sub-networks in the same size logical LUT. All these previous methods train conventional neural networks and convert them to LUTNs; however, research has also been conducted on directly trainable LUTNs. Bacellar *et al.* managed to train both the connections and LUTs in a LUTN they call a Differentiable Weightless Neural Network (DWN) [18]. They utilize an extended finite difference method to train the LUT. However, their representation does not remain true to the boolean operation of the MUX. The difference between this work and [18], is the way the LUTs are trained. Our work uses a boolean equation representing a MUX, which is the actual hardware element behind the LUT. This represents a closer representation of the building blocks in reconfigurable hardware. Gerlach *et al.* continue on the works of the original LGNs and Gumbel LGNs towards an algorithm called Walsh-Assisted Relaxation for Probabilistic Look-Up Tables (WARP-LUTs) [19]. These are networks of 2-input LUTs that are trained with backpropagation, but require fewer parameters and training time compared to LGNs and Gumbel LGNs. As of the time of writing, higher input LUTs have not been tried out using this method.

III. METHODOLOGY

In this section, we will first describe the data set and which data is used for training and testing. Following this, we explain the novel preprocessing method for extracting the features that

TABLE II: n represents the number of inputs of a LUT and # binary functions indicates how many binary functions that LUT can represent.

Type	# binary functions
2-LUT	16
4-LUT	65 536
6-LUT	$1.845 \cdot 10^{19}$
n -LUT	2^{2^n}

are the inputs to the model. Subsequently, we describe the training method for LGNs and how rate coding is applied to improve performance. Next, the training method of the LUTNs is delineated. Finally, we describe the evaluation metrics used in this work.

A. Preprocessing

1) *MIT-BIH data set*: The data set contains 48 two-channel ECG recordings, each about 30 minutes long, originating from 47 patients. This comes down to approximately 50000 heartbeats, containing both normal heartbeats and different arrhythmias [2]. The signal was digitized at a sample rate of 360 Hz and a resolution of 11 bits. We will only use one channel and leave out certain parts of the data as explained in the next subsection.

2) *Train-test split*: The dataset was split into a train set (DS1) and test set (DS2) according to the inter-patient scheme designed by [4]:

- DS1: 101, 106, 108, 109, 112, 114, 115, 116, 118, 119, 122, 124, 201, 203, 205, 207, 208, 209, 215, 220, 223, 230
- DS2: 100, 103, 105, 111, 113, 117, 121, 123, 200, 202, 210, 212, 213, 214, 219, 221, 222, 228, 231, 232, 233, 234

Here, each number designates a patient recording, where only the first channel of the two-channel signal is used. As proposed by the Association for the Advancement of Medical Instrumentation (AAMI), patient records containing paced beats (102, 104, 107, 217) are removed [26]. Additionally, beats are grouped together according to the AAMI guidelines [26]:

$$\begin{aligned}
 N, L, R \rightarrow N & \quad (89\,474 = 45\,626 + 43\,848) \\
 e, j, A, a, J, S \rightarrow S & \quad (6\,986 = 3\,778 + 3\,208) \\
 V, E \rightarrow V & \quad (3\,018 = 975 + 2\,043) \\
 F \rightarrow F & \quad (801 = 413 + 388) \\
 Q,f \rightarrow Q & \quad (15 = 8 + 7).
 \end{aligned}$$

Following these guidelines as in [27], [3], [28], the Q class is ignored, since there are only 15 examples in the data set (8 train examples and 7 test examples). This results in a four-class classification problem: normal heartbeats (N), supraventricular ectopic beats (S or SVEB), ventricular ectopic beats (V or VEB), and beats resulting from the fusion of VEBs and normal beats (F) [4].

3) Feature extraction: A binary feature vector of length 138 is constructed containing the following parameters:

$$\begin{aligned} & [RR_1, RR_2, RR_3, RR_4, \Delta RR_p, \Delta RR_m, \\ & RR_{locCV}, RR_{ratio}, t_b, M_1, M_2, M_4, cf_1, cf_2, \delta]. \end{aligned} \quad (2)$$

Each of these features is explained in the following paragraphs.

First, for each peak position R_0 , the next peak position R_{p1} and three previous peak positions R_{m1} , R_{m2} and R_{m3} are extracted (see Fig. 1). Using these peak positions the RR-intervals [3], [8] RR_1 , RR_2 , RR_3 and RR_4 can be determined. Each of the intervals is encoded into 8-bit binary numbers. The features ΔRR_p and ΔRR_m designate the RR-interval changes [8] and are simply sign bits:

$$\begin{aligned} \Delta RR_p &= \begin{cases} 1 & \text{if } RR_1 > RR_2 \\ 0 & \text{otherwise} \end{cases} \\ \Delta RR_m &= \begin{cases} 1 & \text{if } RR_2 > RR_3 \\ 0 & \text{otherwise.} \end{cases} \end{aligned}$$

Inspired by [3], the local RR interval is determined, specifically RR_2 of $n = 500$ previous examples is calculated. Following this, the mean m and standard deviation s of this list of numbers are calculated to obtain the coefficient of variation m/s . To save power, this value is updated for each heartbeat, rather than calculating it fully from scratch every time. m/s is converted to binary numbers by using thresholds of 0.5 and 0.1 to obtain a two-bit feature RR_{locCV} for each heartbeat. Additionally, the RR-ratio $RR_{ratio} = RR_1/m$ is calculated and converted to 2 binary values by using thresholds of 0.25 and 0.5 to see if this value lies below these thresholds.

Another feature to be extracted is a tachycardia bit t_b , to check if the current selected heartbeat occurs at a rate faster than 100 bpm, which is determined using the local RR-interval.

Hereafter, morphological features are extracted in a similar way to [3]:

- $M_1 = |\text{ecg}[R_0] - \min(\text{beat}[0:40])|/\text{norm}$
- $M_2 = |\text{ecg}[R_0] - \min(\text{beat}[65:85])|/\text{norm}$
- $M_3 = |\text{ecg}[R_0] - \min(\text{beat}[95:105])|/\text{norm}$
- $M_4 = |\text{ecg}[R_0] - \min(\text{beat}[150:180])|/\text{norm}$

Here, ecg is the array containing the values of a patient's recording, beat is an array containing 180 values around the center peak R_0 representing one heartbeat, and $\text{norm} = \max(\text{beat}) - \min(\text{beat})$. For the final feature vector, M_3 is excluded, as the results were better without it. All these features are encoded into 3 bits.

Additionally, the crest factor is determined for better distinguishing normal beats from ventricular ectopic beats, and is defined as the peak amplitude divided by the RMS value of the complete heartbeat. The crest factor cf_1 is determined for a window of 180 samples (as previously done), and cf_2 for a window of 400 samples centered at R_0 .

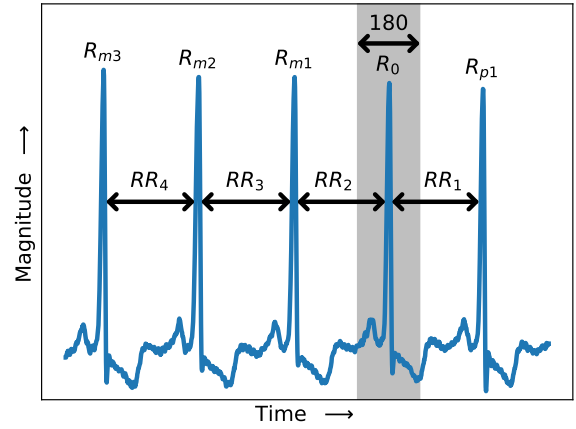


Fig. 1: Excerpt of the ECG data highlighting some of the features to be extracted for the heartbeat that is indicated in gray.

Each crest factor is encoded into 8 bits.

Finally, delta encoding is applied as in [8], obtaining 74 binary numbers represented by δ .

B. Logic gate networks

The LGNs were trained in the same manner as described in [11] with fixed connections and a learning rate of 0.01. All networks had 8000 gates per layer and were trained for 200 epochs using a batch size of 100. An example of an LGN is illustrated in Fig. 2, which shows the binary inputs, feedforward gate network, and population counts for the different classes at the output. While training, the gate types are learned using the differentiable expressions from Table I. In practice, the inputs to the LGNs are binary values; however, in these expressions, x_0 and x_1 can be seen as independent probabilities as mentioned in [11], [22]. Since x_0 and x_1 are probabilities of the inputs being equal to 1, the output of the gate can then again be seen as a probability of being equal to 1. Therefore, during training, it is not needed to convert the inputs into bit streams; we can just propagate full-precision values between 0 and 1 that represent infinitely long bit streams using rate coding. This method not only makes training very fast compared to using bit streams, but it also ensures that the model achieves the best possible performance when using rate coding. Of course, during inference, one has to use finite-length bit streams, resulting in a slightly lower performance depending on the length of the bit stream. In the limit of infinitely long bit streams, the discrete logic gate operations will converge to f_i . The *full precision* feature values of (2) were used as inputs for the rate-coded networks. Furthermore, an additional RR ratio, RR_2/m , is added, resulting in 89 input features. For the non-rate-coded networks, the conventional way of training these networks was employed, using the *binary* input vector (2).

C. LUT networks

The method for training the LUTNs is based on the fact that a LUT in an FPGA is implemented as a MUX. As an example, the boolean equation of an 8:1 MUX is given by the following equation:

$$L_{out} = W_0 \overline{L_0} \overline{L_1} \overline{L_2} + W_1 \overline{L_0} \overline{L_1} L_2 + \dots + W_7 L_0 L_1 L_2. \quad (3)$$

Here L_{out} is the output of the MUX, W_0, \dots, W_7 are the inputs of the MUX, and L_0, L_1 and L_2 are the selector bits. Alternatively, this can also be viewed as a 3-input LUT, where the values of L_0, L_1 , and L_2 determine which of the eight possible LUT outputs W_0, \dots, W_7 is selected to produce the output L_{out} . The equivalence between a LUT and a MUX is given in Fig. 3. Note that this formula is differentiable; hence, backpropagation can be used to find all LUT output values.

In general, an N -input LUT is represented by an $2^N:1$ MUX. The generalized formula for an N -input LUT is given by

$$L_{out} = \sum_{i=0}^{2^N-1} W_i \prod_{j=0}^{N-1} (s_{ij} \overline{L_j} + s_{ij} L_j) \quad (4)$$

$$= \sum_{i=0}^{2^N-1} W_i p(W_i | L_1, \dots, L_{N-1}), \quad (5)$$

$$= \mathbb{E}(\mathbf{W}) \quad (6)$$

$$\text{with } \mathbf{s} = \begin{pmatrix} 0 & 0 & \dots & 0 & 0 \\ 0 & 0 & \dots & 0 & 1 \\ 0 & 0 & \dots & 1 & 0 \\ \vdots \\ 1 & 1 & \dots & 1 & 1 \end{pmatrix}. \quad (7)$$

Here, W_i are the trainable weights, which are the outputs of the LUT. The values of W_i are continuous and are binarized layer-wise during training as in [10]. As can be seen from the sum in this equation, an N -input LUT contains $2^N - 1$ entries, starting from zero. L_j with $j = 0, \dots, N - 1$ are the inputs of the LUT. L_{out} is the LUT output that is selected based on the

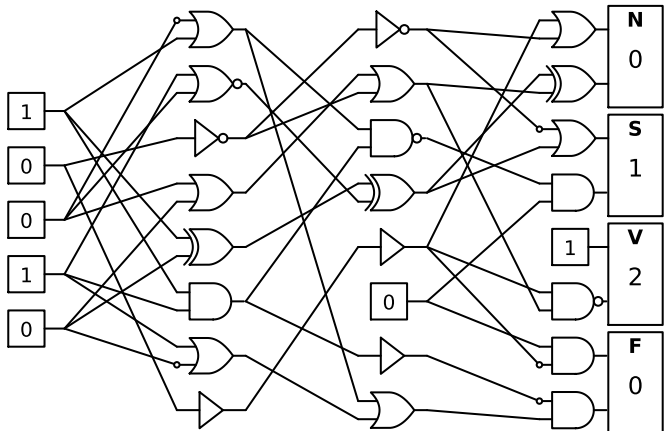


Fig. 2: An example of a 3-layer LGN.

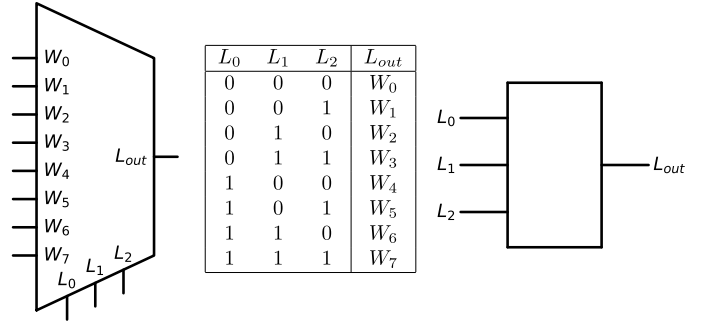


Fig. 3: Equivalence between an 8:1 MUX and a 3-input LUT.

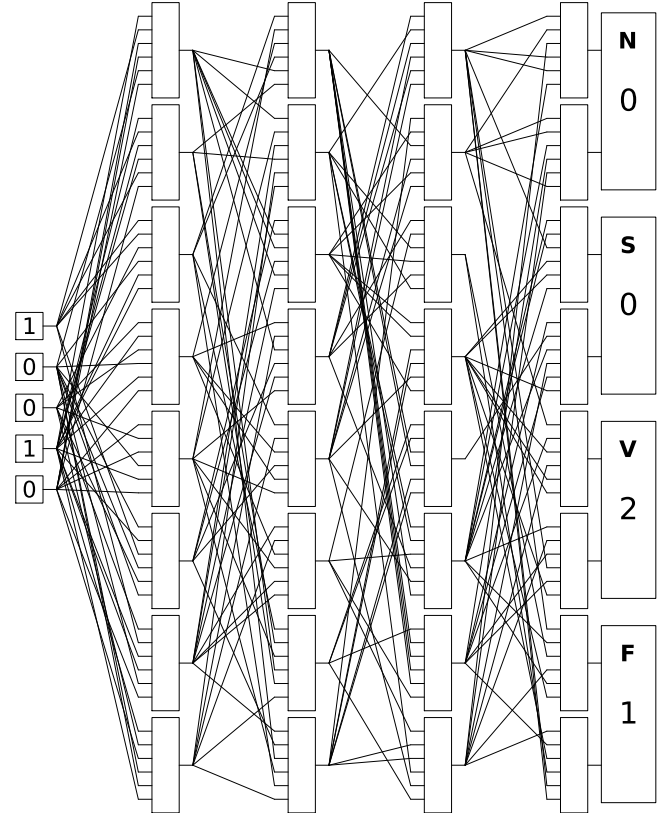


Fig. 4: An example of a 4 layer 6-LUTN.

values of the inputs L_j . In this general formula, the selector matrix s is used to select the correct boolean variables \overline{L}_j or L_j for each j and each LUT output index i . Looking carefully at s , it can be seen that it simply lists values 0 through $N - 1$ in binary format, as is typically observed when writing down truth tables or LUTs. The inputs L_j can also be continuous, representing the probability of the input being equal to one, so these values lie between 0 and 1, meaning that the products of these values (and their inverses) also lie between 0 and 1. Hence, all of the products in (4) lie between 0 and 1. In addition, the sum of all the products in (4) lies between 0 and 1, as can be proven by induction. Consequently from (4) to (5), we can define a probability to obtain (6). During training, one must consider the batch size and the number of LUTs per layer, so that the above L_{out} variable becomes a matrix. The PyTorch pseudo-code for training a layer of LUTs using

the above method is presented in Algorithm 1. Here B is the batch size, I is the input size of a layer, O is the output size of a layer, and N is the number of inputs of a LUT.

Algorithm 1 Forward pass of a LUTN layer

Require: $\text{dim}(\text{input}) = B \times I$

Require: $\text{dim}(\text{idx}) = O \times N$

Require: $\text{dim}(W) = 2^N \times O$

Require: $\text{dim}(s) = 2^N \times N$

Ensure: L_{out} is calculated according to (4)

```

 $L \leftarrow \text{input}[:, \text{idx}].\text{unsqueeze}(2)$ 
 $L \leftarrow \text{broadcast\_to}(L, (B, O, 2^N, N))$ 
 $L \leftarrow \text{torch.prod}(L \cdot s + (1 - L)(1 - s), \text{dim} = -1)$ 
 $L \leftarrow \text{torch.transpose}(L, 1, 2)$ 
 $L_{\text{out}} \leftarrow \text{torch.sum}(L \cdot W, \text{dim} = 1)$ 
return  $L_{\text{out}}$ 

```

D. Evaluation metrics

Accuracy may not be the best evaluation metric for the MIT-BIH data set, as 89.21% of the test data examples are normal heartbeats. This class imbalance means that any classifier that predicts every heartbeat as normal already has an accuracy of 89.21%. Hence, a different metric called the $j\kappa$ index has been proposed for this [27], [3]. The $j\kappa$ index consists of the j index and the Cohen's Kappa index κ as follows:

$$j\kappa = 1/8 \cdot j + 1/2 \cdot \kappa. \quad (8)$$

To make sure that $j\kappa \in [0, 1]$ the values $1/8$ and $1/2$ are chosen, since $j \in [0, 4]$ and $\kappa \in [0, 1]$. The j index is given by [27]:

$$j \text{ index} = SEN_S + SEN_V + PPV_S + PPV_V, \quad (9)$$

and tries to quantify the distinction between the S class and V class, since these are the most important types of arrhythmias. The κ index is given by [29], [3]

$$\kappa = \frac{\text{Acc} - p_e}{1 - p_e}, \quad (10)$$

where Acc is the overall accuracy and p_e is the chance agreement [29], [3]:

$$p_e = \frac{\sum_k \left[\sum_i C_{ik} \cdot \sum_j C_{kj} \right]}{\left(\sum_{ij} C_{ij} \right)^2}, \quad (11)$$

where C is the confusion matrix. The κ index is a more robust metric for imbalanced data sets compared to just the overall or mean accuracy [29], [3].

To make sure that the rate-coded LGNs work as intended, we first benchmark them on the MNIST and Fashion-MNIST data sets. These data sets are often used to test models; they considered as the “Hello, World!” of novel AI models. The MNIST data set contains 28x28 grayscale images of handwritten digits ranging from 0 to 9. Fashion-MNIST is a slightly

more difficult data set, also containing 10 classes of 28x28 grayscale images, but this time the images represent clothing items. The LUTN training method is also tested on these data sets, but only for non-rate-coded input values. Afterwards the LGNs and LUTNs are benchmarked on the MIT-BIH data set using binary input values and full precision rate-coded input values, and are compared against SOTA models based on accuracy, $j\kappa$ -index and number of FLOPs per inference. To estimate the number of FLOPs for the LGNs, we use the conservative estimate of 100 binary (i.e. gate) operations for one floating point operation as mentioned in [11]. In reality, it is expected that one FLOP requires much more than 100 gate operations, and as such, the number of FLOPs for the LGNs (and by extension the LUTNs) should be lower. The number of FLOPs for the LUTNs is calculated in the same manner, taking into account that an N-LUT is represented by a $2^N:1$ MUX that contains $3(2^N - 1)$ gates. To estimate the FLOPs of the readout, the number of gates for an adder tree is counted and converted to FLOPs. Finally, we estimate the number of LUTs and power usage on an FPGA for the LGNs and LUTNs, and compare these to SOTA LGN models.

IV. RESULTS

A. Rate coding of LGNs

To evaluate the effect of rate-coding LGNs, the networks were tested on the MNIST and Fashion-MNIST datasets for different network depths, using 8000 gates per layer. These findings are displayed in Fig. 5a (MNIST) and 5b (Fashion-MNIST), and are compared to traditional single threshold-coded LGNs. From these results, it can be concluded that all rate-coded networks outperform the thresholded ones on both data sets. The results of using rate coding for the MIT-BIH data set are presented in Section IV-D, along with the performance of the other models on this data set.

B. LUTN training method

To ensure that the LUTN training method works effectively, it is first tested on the MNIST and Fashion-MNIST data sets. Table III gives the accuracy of an LGN (8000 gates/layer), 2-LUTN (8000 gates/layer), 4-LUTN (3000 gates/layer), and 6-LUTN (2000 gates/layer). This means that the 4-LUTNs and 6-LUTNs have only 12000 connections, while the LGNs and 2-LUTNs have 16000. Although the 6-LUTNs have fewer connections compared to the LGNs, they always have the best performance, due to the exponential number of functions that a LUT can represent (Table II). However, for the last entry, the 6-LUTN performs worse. We suspect that the LUTN training algorithm performs worse for deep networks and a high number of inputs per LUT, since this results in a lot of multiplications of small numbers, as can be seen from equations (3), (4), and (7). Finding the exact reason for this behavior would require further investigation. Furthermore, the LGNs and 2-LUTNs exhibit similar performance, which is understandable since they are both networks of logic gates, albeit trained in different manners. The performance of the 4-LUTNs is somewhere between the LGNs and 6-LUTNs, because the size of the 4-LUT function space is between the size of the function spaces of 2-LUTs and 6-LUTs.

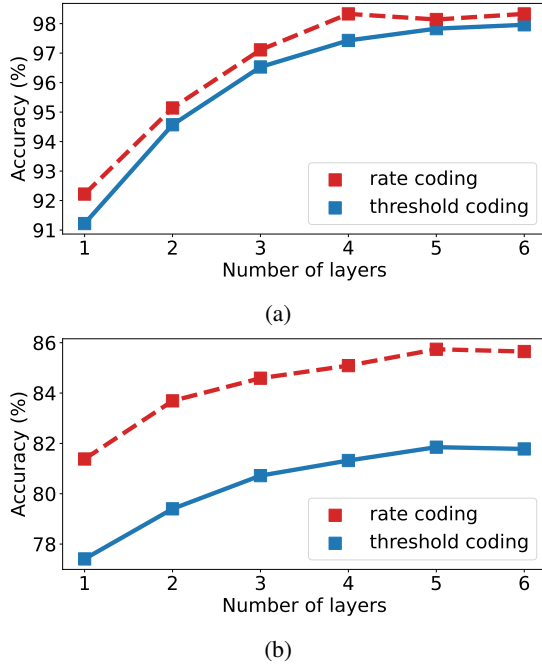


Fig. 5: Comparison between single threshold coding and rate coding on the MNIST data set (a) and Fashion-MNIST data set (b), for LGNs using 8000 gates per layer.

TABLE III: Accuracies (%) of the LGNs [11] and LUTNs (ours) on the MNIST and Fashion-MNIST data set.

Model	MNIST		Fashion-MNIST	
	1 layer	2 layers	1 layer	2 layers
LGN [11]	91.22	94.57	77.41	79.40
2-LUTN	92.21	94.29	76.91	77.92
4-LUTN	93.11	96.73	77.91	79.28
6-LUTN	94.13	97.24	78.72	77.67

C. ECG arrhythmia classification: Mixed patients

Table IV gives the accuracy on the ECG test set using LGNs when patients are mixed. In all experiments, the networks were trained for 200 epochs using 8000 gates per layer. Here, a random train-test split of 0.67–0.33 was used. The reported accuracies of [30] are 97.54%, 97.86% and 98.05%, respectively, but under previously mentioned training circumstances, the accuracies are lower, as can be seen in Table IV. As mentioned in III-A, 4 classes were used in all of our models, since the fifth class only consists of 15 examples. It can be concluded that our preprocessing method significantly increases the accuracy on the ECG data set. Table V gives the ideal temperature of the softmax of the output layer.

D. ECG arrhythmia classification: Inter-patient paradigm

The results of applying the inter-patient paradigm to the MIT-BIH data set using LGNs and LUTNs are presented in Tables VI and VII. The LGNs, 4-LUTNs, and 6-LUTNs use 8000 gates/layer (16000 connections), 3000 LUTs/layer (12000 connections), and 2000 LUTs/layer (12000 connections) respectively. Both binary features and numerical features (rate-coded) are tested. In addition, our results are compared to those of the LGNs in [30], which

TABLE IV: Accuracy (%) results for the mixed patients case (LGNs). The second and third columns use the binary and numerical features described in this work respectively. The superscript r indicates the use of rate coding as described in this work. The last column only uses dynamic thresholds as preprocessing [30].

# layers	LGNs (ours)	LGNs ^r (ours)	LGNs [30]
2	97.90	97.56	97.10
3	98.25	97.64	97.30
4	98.35	97.76	97.44

TABLE V: Ideal temperatures for the networks that use mixed patients.

Temperature	LGNs	LGNs ^r	[30] (4 classes)	[30] (5 classes)
	30	20	8	5

used only dynamic thresholds for preprocessing. From these results, it can be concluded that using just thresholds is not enough for performing well on this data set, e.g. the normal class occurs 89.21% of the time, which should be the lower bound of the accuracy, and the networks of [30] do not perform that much better. On the other hand, using our preprocessing method, all networks achieve an accuracy above 94%. For the $j\kappa$ -index the same story holds, just using thresholds does not give a high enough performance using the inter-patient paradigm. The most important metric of the two is the $j\kappa$ -index, which is highest for a rate-coded 2-layer LGN. To actually implement such an LGN, bit streams of finite length are necessary. Fig. 6 gives the accuracy and $j\kappa$ -index of this network on the whole test set as a function of the number of time steps (i.e. bit stream length). As expected, the lower the bit stream length, the lower the performance. Looking back at Tables VI and VII, one can also see that the rate-coded LUTNs perform worse than the non-rate-coded ones. Why that is the case is not entirely clear, since inputs and outputs are between 0 and 1, according to (6), which represents rates. It is possible that before binarization, the output is not necessarily between 0 and 1, which can cause issues during training. Additionally, deep 6-LUTNs perform quite badly due to multiplying many small numbers, as explained in section IV-B. Table VIII gives the optimal output softmax temperature of the different models. Table X and Table XI compare our approaches with SOTA approaches in terms of accuracy and $j\kappa$ -index respectively. In terms of accuracy, only an ensemble of SVMs performs better. Examining the $j\kappa$ -index, the SVM and the deep residual CNN yield the best results.

With the goal of assessing the power consumption of our networks, we estimate the number of FLOPs (per inference). Table IX shows the results for the top-performing SOTA models and an SNN. Although the SVM has the best performance, the LGNs and LUTNs require about three orders of magnitude less FLOPs. As mentioned before, it is expected that the number of FLOPs for the LGNs and LUTNs are significantly lower, due to our conservative conversion from gates to FLOPs. Additionally, the number of FLOPs for the

TABLE VI: Accuracies (%) of our networks (LGNs, 4-input LUTNs, and 6-input LUTNs) that use the inter-patient paradigm. The superscript r indicates the use of rate coding as described in this work. This is compared to state-of-the-art LGNs on this data set.

# layers	LGNs	LGNs ^r	4-LUTNs	4-LUTNs ^r	6-LUTNs	6-LUTNs ^r	LGNs [30]
1	93.79	93.63	94.00	92.91	94.04	92.66	90.86
2	94.06	93.48	94.26	92.85	94.24	92.79	90.30
3	94.19	93.50	94.21	93.14	94.20	93.17	89.73
4	94.28	93.26	94.23	93.20	88.67	92.14	91.13

TABLE VII: $j\kappa$ -indexes of our networks (LGNs, 4-input LUTNs and 6-input LUTNs) that use the inter-patient paradigm. The superscript r indicates the use of rate coding as described in this work. This is compared to state-of-the-art LGNs on this data set.

# layers	LGNs	LGNs ^r	4-LUTNs	4-LUTNs ^r	6-LUTNs	6-LUTNs ^r	LGNs [30]
1	0.645	0.633	0.646	0.549	0.651	0.572	0.398
2	0.569	0.683	0.638	0.614	0.643	0.571	0.425
3	0.650	0.660	0.624	0.557	0.583	0.561	0.441
4	0.559	0.649	0.635	0.612	0.000	0.000	0.410

TABLE VIII: Ideal temperatures for the networks that use the inter-patient paradigm.

	LGNs	LGNs ^r	4-LUTNs	4-LUTNs ^r	6-LUTNs	6-LUTNs ^r	[30]
Temperature	35	10	30	40	25	15	30

TABLE IX: Comparison of the number of floating-point operations per inference (FLOPs) for different approaches. The accuracy and $j\kappa$ -index are also added. The total number of FLOPs is the sum of the FLOPs for preprocessing, the network, and the readout. Only the convolution operations are counted for the ANN, and no preprocessing FLOPs are counted for the SVM.

Model	Architecture	FLOPs preproc.	FLOPs network	FLOPs readout	FLOPs total	Acc.	$j\kappa$	Reference
LGNs	1x8k	2246	80	560	2.89 K	94.28	0.645	Ours
2-LUTNs	1x8k	2246	720	560	3.53 K	94.28	0.645	Ours
4-LUTNs	1x3k	2246	1350	211	3.81 K	94.26	0.646	Ours
6-LUTNs	1x2k	2246	3780	139	6.17 K	94.24	0.651	Ours
SVM	Ensemble	-	$4.93 \cdot 10^6$	0	> 4.93 M	94.50	0.773	[3]
SNN	Conv.	0	$31.0 \cdot 10^6$	-	31.0 M	90.00	0.636	[9]
ANN	Conv.	-	$1.35 \cdot 10^9$	0	> 1.35 G	88.99	0.701	[5]

TABLE X: Comparison of different SOTA approaches based on accuracy.

Model	Accuracy (%)	Reference
Ensemble of 6 SVMs	94.50	[3]
LGN	94.28	Ours
4-LUTN	94.26	Ours
6-LUTN	94.24	Ours
SNN	93.67	[8]
LGN ^r	93.63	Ours
SNN ^r + CNN	90.00	[9]
SNN ^r + SNN ^r	90.00	[9]
Deep residual CNN	88.99	[5]
LS-SVM	81.00	[6]

preprocessing is mainly dominated by the calculation of the crest factor.

E. FPGA implementation

Power estimations for different networks are shown in Fig. 7a. These networks were simulated in both Xilinx Vivado and Cadence Excelium. The latter was used to obtain the activity files that are loaded into Vivado to estimate the power. Our networks consume a power between 5 mW and 7 mW without preprocessing and readout, and only require one clock cycle of 10 ns to compute the output, which amounts to an energy of 50 pJ to 70 pJ per inference. In this figure, the best-performing network in terms of accuracy, as reported in [30],

TABLE XI: Comparison of different SOTA approaches based on $j\kappa$ -index.

Model	$j\kappa$ -index	Reference
Ensemble of 6 SVMs	0.773	[3]
Deep residual CNN	0.701	[5]
LGN ^r	0.683	Ours
SNN ^r + CNN	0.672	[9]
6-LUTN	0.651	Ours
4-LUTN	0.646	Ours
LGN	0.645	Ours
SNN ^r + SNN ^r	0.636	[9]
LS-SVM	0.610	[6]

is the 4-layer network. Our networks have a higher accuracy and $j\kappa$ -index, but a lower power usage compared to that network, and as such perform better in every aspect, except for preprocessing FLOPs. The same networks are synthesized in Vivado to determine the number of LUTs, which can be found in Fig. 7b. Again, our networks outperform those in [30] in terms of the number of LUTs. In addition, the hyperparameter in PyTorch that specified the number of 6-LUTs per layer was set to 2000, which is exactly the number of LUTs in the final implementation of the 6-LUTN, showcasing that there is indeed a one-to-one mapping from software to hardware. These results were estimated using an Artix 7 low-voltage FPGA (part number xc7a12tclcp238-2L). A similar experiment was performed for the 1-layer and 2-layer rate-

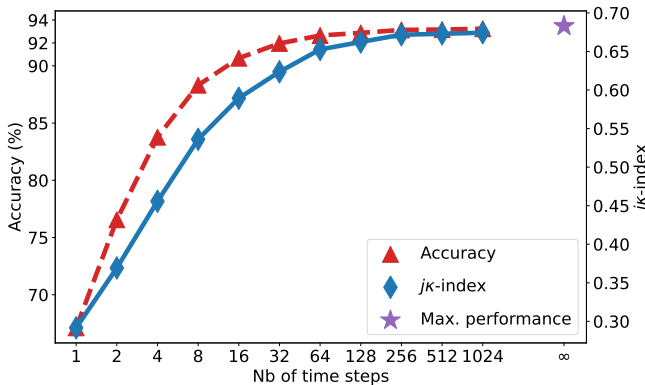
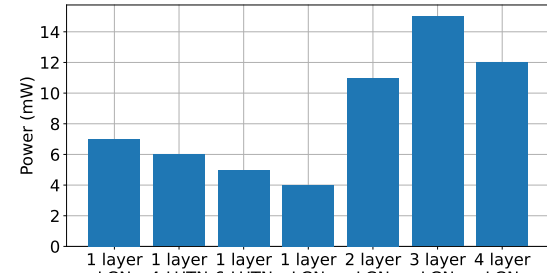


Fig. 6: The accuracy (dashed line) and $j\kappa$ -index (solid line) of the 2-layer rate-coded LGN as a function of the number of timesteps. The star indicates the best value that can be reached for both accuracy and $j\kappa$ -index.

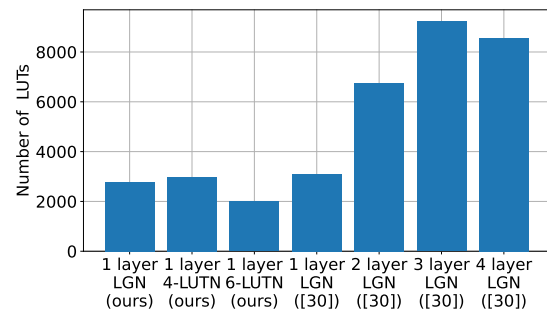
coded LGNs, with a sequence length of 128. Since each output gate now has an 8-bit counter attached to it to count the number of spikes or ones over all 128 timesteps, the power and number of LUTs are significantly higher. The results on an Artix UltraScale+ FPGA (part number xcau7p-fcva289-1LV-i) for a 1-layer and 2-layer network were 133 mW using 33526 LUTs and 271 mW using 53476 LUTs. Hence, the small increase in performance likely does not justify the large increase in LUTs and power consumption.

V. CONCLUSION

We show that the LGNs and LUTNs can be used for ECG arrhythmia classification using the inter-patient paradigm. It was demonstrated that rate-coded LGNs outperform LGNs with only threshold coding. Additionally, it was demonstrated that the novel LUTN training method is effective for the MNIST, Fashion-MNIST, and MIT-BIH arrhythmia datasets. Using a new preprocessing method, improvements can be made to the mixed-patient and inter-patient paradigms of the ECG dataset. Using a 4-layer LGN, a mixed-patient accuracy of 98.35% was achieved. Utilizing the inter-patient paradigm, accuracies above 94% could be achieved for the LGNs and LUTNs. The highest $j\kappa$ -index for these types of networks was 0.683. Additionally, FPGA power and area estimations showed that our models have a lower energy usage and a lower number of LUTs compared to SOTA LGNs, while still having a significantly higher accuracy and $j\kappa$ -index. The rate-coded networks showed a significant increase in power, latency, and area, making it better to use the normal binary encoding. Finally, compared to general SOTA methods, the LGNs and LUTNs perform quite well. Only an ensemble of SVMs and a deep residual CNN performs better, since they require an estimated three to six orders of magnitude more FLOPs. To further improve the models and address the class imbalance, we could utilize a focal loss [31] and synthetic minority oversampling (SMOTE) [32]. Finally, LGNs and LUTNs are good candidates as wake-up systems for more complex classifiers, due to their simple implementation and low power consumption.



(a)



(b)

Fig. 7: (a) Power estimation and (b) number of LUTs of an Artix 7 low-voltage FPGA (part number xc7a12tlcp238-2) using our LGN, 4-LUTN and 6-LUTN networks compared to [30]

REFERENCES

- [1] World Health Organization (WHO), “Cardiovascular diseases.” <https://www.who.int/health-topics/cardiovascular-diseases>, 2025.
- [2] G. Moody and R. Mark, “The impact of the MIT-BIH Arrhythmia Database,” *IEEE Engineering in Medicine and Biology Magazine*, vol. 20, pp. 45–50, May 2001.
- [3] V. Mondéjar-Guerra, J. Novo, J. Rouco, M. G. Penedo, and M. Ortega, “Heartbeat classification fusing temporal and morphological information of ECGs via ensemble of classifiers,” *Biomedical Signal Processing and Control*, vol. 47, pp. 41–48, Jan. 2019.
- [4] P. de Chazal, M. O’Dwyer, and R. Reilly, “Automatic classification of heartbeats using ECG morphology and heartbeat interval features,” *IEEE Transactions on Biomedical Engineering*, vol. 51, pp. 1196–1206, July 2004.
- [5] Y. Li, R. Qian, and K. Li, “Inter-patient arrhythmia classification with improved deep residual convolutional neural network,” *Computer Methods and Programs in Biomedicine*, vol. 214, p. 106582, Feb. 2022.
- [6] A. Villa, M. Deviae, R. Willems, S. Van Huffel, and C. Varon, “Are we training our heartbeat classification algorithms properly?,” *IEEE Engineering in Medicine and Biology Society*, vol. 2019, pp. 6363–6366, July 2019.
- [7] B. Hawks, J. Duarte, N. J. Fraser, A. Pappalardo, N. Tran, and Y. Umuroglu, “Ps and Qs: Quantization-Aware Pruning for Efficient Low Latency Neural Network Inference,” *Frontiers in Artificial Intelligence*, vol. 4, July 2021.
- [8] R. Mao, S. Li, Z. Zhang, Z. Xia, J. Xiao, Z. Zhu, J. Liu, W. Shan, L. Chang, and J. Zhou, “An Ultra-Energy-Efficient and High Accuracy ECG Classification Processor With SNN Inference Assisted by On-Chip ANN Learning,” *IEEE transactions on biomedical circuits and systems*, vol. 16, pp. 832–841, Oct. 2022.
- [9] Z. Yan, J. Zhou, and W.-F. Wong, “Energy efficient ECG classification with spiking neural network,” *Biomedical Signal Processing and Control*, vol. 63, p. 102170, Jan. 2021.
- [10] L. Keuninckx, M. Hartmann, P. Detteler, A. Safa, W. Mommen, and I. Ocket, “On Training Networks of Monostable Multivibrator Timer Neurons,” *Neural Networks*, p. 108092, Sept. 2025.

- [11] F. Petersen, C. Borgelt, H. Kuehne, and O. Deussen, “Deep Differentiable Logic Gate Networks,” *Advances in Neural Information Processing Systems*, vol. 35, pp. 2006–2018, Dec. 2022.
- [12] E. Wang, J. J. Davis, P. Y. K. Cheung, and G. A. Constantinides, “LUTNet: Rethinking Inference in FPGA Soft Logic,” Apr. 2019.
- [13] E. Wang, J. J. Davis, P. Y. K. Cheung, and G. A. Constantinides, “LUTNet: Learning FPGA Configurations for Highly Efficient Neural Network Inference,” Mar. 2020.
- [14] Y. Umuroglu, Y. Akhauri, N. J. Fraser, and M. Blott, “LogicNets: Co-Designed Neural Networks and Circuits for Extreme-Throughput Applications,” in *2020 30th International Conference on Field-Programmable Logic and Applications (FPL)*, pp. 291–297, Aug. 2020.
- [15] M. Nazemi, G. Pasandi, and M. Pedram, “Energy-Efficient, Low-Latency Realization of Neural Networks Through Boolean Logic Minimization,” in *2019 24th Asia and South Pacific Design Automation Conference (ASP-DAC)*, pp. 1–6, Jan. 2019.
- [16] M. Andronic and G. A. Constantinides, “PolyLUT: Learning Piecewise Polynomials for Ultra-Low Latency FPGA LUT-based Inference,” in *2023 International Conference on Field Programmable Technology (ICFPT)*, pp. 60–68, Dec. 2023.
- [17] M. Andronic and G. A. Constantinides, “NeuraLUT: Hiding Neural Network Density in Boolean Synthesizable Functions,” in *2024 34th International Conference on Field-Programmable Logic and Applications (FPL)*, pp. 140–148, Sept. 2024.
- [18] A. T. L. Bacellar, Z. Susskind, M. B. Jr, E. John, L. K. John, P. M. V. Lima, and F. M. G. França, “Differentiable Weightless Neural Networks,” Nov. 2024.
- [19] L. Gerlach, L. Våge, T. Gerlach, and E. Kauffman, “WARP-LUTs - Walsh-Assisted Relaxation for Probabilistic Look Up Tables,” Oct. 2025.
- [20] W. Maass, “Networks of spiking neurons: The third generation of neural network models,” *Neural Networks*, vol. 10, pp. 1659–1671, Dec. 1997.
- [21] S. Bührer, A. Plesner, T. Aczel, and R. Wattenhofer, “Recurrent Deep Differentiable Logic Gate Networks,” Aug. 2025.
- [22] F. Petersen, H. Kuehne, C. Borgelt, J. Welzel, and S. Ermon, “Convolutional Differentiable Logic Gate Networks,” Nov. 2024.
- [23] W. Mommen, L. Keunincx, M. Hartmann, and P. Wambacq, “A Method for Optimizing Connections in Differentiable Logic Gate Networks,” July 2025.
- [24] S. Yousefi, A. Plesner, T. Aczel, and R. Wattenhofer, “Mind the Gap: Removing the Discretization Gap in Differentiable Logic Gate Networks,” June 2025.
- [25] M. Rastegari, V. Ordonez, J. Redmon, and A. Farhadi, “XNOR-Net: ImageNet Classification Using Binary Convolutional Neural Networks,” Aug. 2016.
- [26] *Testing and Reporting Performance Results of Cardiac Rhythm and ST Segment Measurement Algorithms*. Association for the Advancement of Medical Instrumentation, 1998.
- [27] T. Mar, S. Zaunseder, J. P. Martínez, M. Llamedo, and R. Poll, “Optimization of ECG Classification by Means of Feature Selection,” *IEEE Transactions on Biomedical Engineering*, vol. 58, pp. 2168–2177, Aug. 2011.
- [28] Z. Zhang, J. Dong, X. Luo, K.-S. Choi, and X. Wu, “Heartbeat classification using disease-specific feature selection,” *Computers in Biology and Medicine*, vol. 46, pp. 79–89, Mar. 2014.
- [29] M. Fatourechi, R. K. Ward, S. G. Mason, J. Huggins, A. Schlägl, and G. E. Birch, “Comparison of Evaluation Metrics in Classification Applications with Imbalanced Datasets,” in *2008 Seventh International Conference on Machine Learning and Applications*, pp. 777–782, Dec. 2008.
- [30] C. Feng, X. Wang, and T. T. Ye, “Low-Power Consumption Inference of ECG Signals Using Differential Logic Networks,” in *2024 IEEE Asia Pacific Conference on Circuits and Systems (APCCAS)*, pp. 20–24, Nov. 2024.
- [31] T.-Y. Lin, P. Goyal, R. Girshick, K. He, and P. Dollár, “Focal Loss for Dense Object Detection,” Feb. 2018.
- [32] N. V. Chawla, K. W. Bowyer, L. O. Hall, and W. P. Kegelmeyer, “SMOTE: Synthetic Minority Over-sampling Technique,” *Journal of Artificial Intelligence Research*, vol. 16, pp. 321–357, June 2002.